

# The CH(G) index as a new criterion for selecting red giant stars

Y.Q. Chen, G. Zhao, K. Carrell, J.K. Zhao and K.F. Tan

## ABSTRACT

We have measured the CH G band (CH(G)) index for evolved stars in the globular cluster M3 based on the SDSS spectroscopic survey. It is found that there is a useful way to select red giant branch (RGB) stars from the contamination of other evolved stars, such as asymptotic giant branch (AGB) and red horizontal branch (RHB) stars, by using the CH(G) index versus  $(g - r)_0$  diagram if the metallicity is known from the spectra. When this diagram is applied to field giant stars with similar metallicity we establish a calibration of  $CH(G) = 1.625(g - r)_0 - 1.174(g - r)_0^2 - 0.934$ .

This method is confirmed by stars with  $[Fe/H] \sim -2.3$  where spectra of member stars in globular clusters M15 and M92 are available in the SDSS database. We thus extend this kind of calibration to every individual metallicity bin ranging from  $[Fe/H] \sim -3.0$  to  $[Fe/H] \sim 0.0$  by using field red giant stars with  $0.4 \leq (g - r)_0 \leq 1.0$ . The metallicity-dependent calibrations give,  $CH(G) = 1.625(g - r)_0 - 1.174(g - r)_0^2 + 0.060[Fe/H] - 0.830$  for  $-3.0 < [Fe/H] \leq -1.2$  and  $CH(G) = 0.953(g - r)_0 - 0.655(g - r)_0^2 + 0.060[Fe/H] - 0.650$  for  $-1.2 < [Fe/H] < 0.0$ . The calibrations are valid for the SDSS spectroscopic data set, and they can not be applied blindly to other data sets. With the two calibrations, a significant number of the contaminating stars (AGB and RHB stars), were excluded and thus a clear sample of red giant stars is obtained by selecting stars within  $\pm 0.05 mag$  of the calibration. The sample is published online and it is expected that this large and clean sample of RGB stars will provide new information on the formation and evolution of the Galaxy.

*Subject headings:* stars: distances – stars: late type – stars: evolution – globular clusters: general – globular clusters: individual (M3, M15, M92) – Galaxy: abundances

## 1. Introduction

Late type stars constitute the most important tracers for understanding the chemical and kinematical evolution of the Galaxy. Among them, unevolved stars, dwarf and subgiant stars, are widely used to probe different stellar populations of the Galaxy in the solar neighborhood. However, evolved stars with bright absolute magnitude are necessary targets to extend the Galactic study far from the solar neighborhood where the Galactic halo is the main population. In this regard, horizontal branch stars with a constant luminosity are the most common stellar tracers and thus are widely used in Galactic halo study. However, we note that the most populated targets of evolved stars in the halo are red giant stars, which will constitute a larger sample of targets for statistical study. In this sense, red giant stars are important stellar tracers for Galactic evolution.

The SDSS and its extensions provide *ugriz* photometry and low resolution spectra for a large amount of Galactic stars, including a huge amount of red giant stars having the main spectral types of G and K (hereafter GK red giants)(Abazajian et al. 2009; Yanny et al. 2009; Aihara et al. 2011; Ahn et al. 2012). There are some works on the Galaxy based on unevolved stars (main-sequence and turnoff stars) of the SDSS spectroscopic survey (Allende Prieto et al. 2006; Carollo et al. 2010; Bond et al. 2010) and a few works adopt later type M giants as stellar tracers (Palladino et al. 2012). As we stated above, unevolved stars reach a smaller distance range than that of evolved stars, and later type M giants mainly represent the metal-rich or young populations (Palladino et al. 2012). Instead, GK red giant stars have the advantage of tracing the metal-poor and old populations of the Galaxy extending to a distance of at least 20 kpc. However, there is no work on Galactic evolution using GK red giant stars as stellar tracers based on the SDSS survey in the literature. Thus, it is of high interest to investigate the chemical and kinematic properties of different populations in the Galaxy by using GK red giant stars from the SDSS spectroscopic survey, which will be the scope of our next paper. It is expected that a large sample of GK red giant stars in the SDSS survey will provide new information on the formation of the halo, the division of the inner and outer halo and the transition from the halo to disk.

Before a statistical study can be carried out, clear selection of red giant stars without contamination of stars from other stages is important. It is known that evolved stars with GK spectral type in the SDSS spectroscopic survey span the entire RGB mixing with the red clump, RHB and early-AGB phases. The contamination of these stars in the RGB sample could affect the spatial, kinematic and chemical distributions in the statistical study. In particular, distances of red giant stars beyond the solar neighborhood are usually estimated from interpreting the fiducial sequence (hereafter FS) of globular clusters (GCs) or isochrones of theoretical models. In this way, wrong distances will be provided for the contaminating

stars (such as red clump, RHB and early-AGB stars) if they are assumed to be RGB stars since they have similar colors but very different luminosities at a given metallicity. In principle, stellar parameters (temperature, gravity and metallicity) from the SSPP (Lee et al. 2008a,b) in the SDSS database can be used to separate evolved and unevolved stars, with  $\log g < 3.5$  being the former. However, since  $\log g$  values provided by the SSPP pipeline have quite large uncertainties, they cannot be used to further classify among evolved stars. In this work, we are searching for the possible criterion for separating the early-AGB and RHB stars from the RGB by using the line index measured from member stars of globular clusters and field stars in the SDSS survey.

## 2. Data and Line Index Measurements

There are eight GCs in the SDSS spectroscopic survey that have enough spectra of member stars for statistical study, and Smolinski et al. (2011a) have presented these cluster stars. For field stars, we select a sample of stars from the SDSS DR9 catalog with a  $(g - r)_0$  range of  $-0.2$  to  $1.0$  mag,  $[\text{Fe}/\text{H}]$  from  $< -2.8$  to  $0.0$  and  $\log g$  less than  $3.5$  dex, where the main targets are giant stars. The sample is limited to stars with spectra available in the DR7 database, but the stellar parameters and  $(g - r)_0$  were taken from the SDSS DR9 database. This limitation of using spectra in DR7 (instead of DR9) will reduce the star number in the field sample, but we assume that there are enough stars in the DR7 database for high statistics.

We have measured the CH(G) index (CH G band at  $\lambda 4300\text{\AA}$ ) defined by Lee (1999) and the spectral index S(3839) (CN band at  $\lambda 3883\text{\AA}$  defined by Norris et al. (1981), following the same definitions adopted in Smolinski et al. (2011b). Note that the released spectra of the SDSS DR7 database are flux calibrated and the wavelength is shifted such that measured velocities will be relative to the solar system barycenter at the mid-point of each 15-minute exposure. We thus corrected the wavelength with the redshift of  $elodierv_z = (elodierv - 7.3)/c$  where  $elodierv$  is taken from the sppParams table of the SDSS DR7 database (in order to fit our spectra from DR7; and we checked that they are generally in agreement with DR9),  $c$  is the speed of light, and  $7.3 \text{ km s}^{-1}$  is an empirically derived offset putting the  $elodierv$  of all stars on a system consistent with that of other literature measures of known radial velocity standards as described in Lee et al. (2008b). Then we interpolate the spectra and produce new spectra with 5,000 points for the wavelength range of  $3840\text{-}4500\text{\AA}$  (versus  $\sim 700$  points in the original spectra) so that the measurements of the line index will not depend on the chosen points at the edge of the defined bands and thus the line index will become more consistent among stars. We have checked that both sets of data generally agree quite

well. Errors are less than 0.03 mag for  $(g - r)_0$  based on  $g$  and  $r$  SDSS photometric errors, less than 0.015 mag for the S(3839) index and less than 0.012 mag for the CH(G) index. To determine the errors on the line index we included errors in the flux (available in the SDSS spectra fits files) and in the wavelength shift (via the radial velocity errors) since these are the two dominant sources of uncertainty in our determination. The comparison of our indices with those of Smolinski et al. (2011b) shows a systematically higher value for the CH(G) index and lower value for the S(3839) index by the order of 0.02 mag in our work with a small scatter of 0.003 mag. The systematic deviation disappears if we adopt the redshift available in the fits file headers. Therefore, the small scatter in the line index comparison indicates a good agreement between Smolinski et al. (2011b) and our work. The wavelength correction by using *elodierv* in our work is more reasonable than using the redshift in the fits file headers since this is the way that the SDSS survey presents its spectra. But both works have internally consistent values for stars and thus this difference will not significantly affect the results.

### 3. Results

#### 3.1. The $(g - r)_0$ versus CH(G) diagram in M3

Among the eight GCs in the SDSS spectroscopic survey, only M3 has a significant number of AGB stars, while others do not have many early-AGB and RHB member stars. Thus we start the study from globular cluster M3 in this work. We adopted the member star list of M3 from Smolinski et al. (2011b) (their Table 3) and obtained photometry and stellar parameters from the SDSS DR9 database (Ahn et al. 2012). With the adopted distance modulus of 15.070 in  $V$  band and reddening of 0.010 from the new version of Harris (1996) published in 2010<sup>1</sup> we calculated the absolute magnitude in  $g$  band ( $M_g = g_0 - 15.070 - 3.1 * 0.010$ ) for each star.

There are 77 member stars in the list of Smolinski et al. (2011b), but we exclude four BHB stars with  $(g - r)_0 < 0.0$  since they are not in the color range of GK red giant stars. Moreover, we found one star with the identification numbers (plate-mjd-fiberid) of 2475-53845-486 is significantly outside the FS of M3, which was excluded as well. Among the remaining 72 member stars, three groups are divided according to their evolutionary stages. There are 12 RHB (open squares), 10 early-AGB (open diamonds) and 50 RGB stars (filled circles), which are shown in Fig. 1. The solid line in the upper-left panel of Fig. 1 shows the

---

<sup>1</sup><http://physwww.mcmaster.ca/harris/mwgc.dat>

observed FS of M3 based on An et al. (2008) and the dash-dotted line shows a theoretical isochrone of 11.5 Gyr, which is close to 11.3 Gyr for M3. Also shown are dotted lines for 8 and 14 Gyr isochrones at  $[\text{Fe}/\text{H}] = -1.5$  from the Dartmouth isochrones (Dotter et al. 2008). It seems that age variation from 8 to 14 Gyr has no significant effect on the CMD and thus it is possible to extrapolate our result to field stars with different ages in the following sections.

The upper-right panel of Fig. 1 shows the CH(G) index as a function of  $(g - r)_0$  with three groups of stars indicated by different symbols. The lower two panels present the S(3839) index as functions of  $(g - r)_0$  and  $M_g$ , and stars with enhanced S(3839) index are indicated by additional pluses in Fig. 1. It is interesting that the RGB is clearly separated from early-AGB stars in the  $(g - r)_0$  versus the CH(G) index diagram despite their similar colors. In the S(3839) vs.  $(g - r)_0$  diagram, RGB stars with  $(g - r)_0 > 0.4 \text{ mag}$  show two branches with a clear gap in between. Early-AGB stars lie in between but are located closer to the lower branch. There is a hint of lower CH(G) indices for S(3839)-strong RGB stars as compared with S(3839)-weak RGB stars, but it is difficult to separate them considering significant scatter in the CH(G) index at a given  $(g - r)_0$  color. With significantly lower  $(g - r)_0$  colors, RHB stars have even lower CH(G) indices due to their higher temperatures. The implication from Fig. 1 is that the CH(G) index is a better criterion than the S(3839) index for excluding early-AGB stars from RGB stars. Moreover, in comparison with the  $T_{\text{eff}}$  versus  $\log g$  diagram in Fig. 2, we can see that the CH(G) index is a more successful way to exclude early-AGB and RHB/BHB stars.

The origin for the lower CH(G) indices for AGB stars than those of RGB stars at similar colors is the so-called weak G-band effect first noted by Zinn (1973). This effect comes from a combination of low carbon abundances and low gravities in the AGB stars (Suntzeff 1981; Briley et al. 1990). The lower carbon abundance in AGB stars than RGB stars at similar colors was theoretically predicted since Sweigart & Mengel (1979) and very recently by Angelou et al. (2011), who proposed a theoretical model of carbon evolution for M3 and showed that carbon abundances decrease after the bump of the RGB due to the onset of extra mixing. With bright luminosities, the early-AGB stars of M3 in our work have lower gravities than RGB stars at similar colors and are in a later stage after the bump of the RGB. Both factors contribute to the significant gap between the early-AGB stars and lower RGB stars in the  $(g - r)_0$  versus CH(G) diagram.

In order to check if the CH(G) index can successfully separate RGB stars from other contaminations at a given metallicity similar to M3, we select a sample of stars from SDSS DR9 with  $0.1 \leq (g - r)_0 \leq 0.8 \text{ mag}$ ,  $-1.6 \leq [\text{Fe}/\text{H}] \leq -1.4 \text{ dex}$  and  $\log g < 3.5 \text{ dex}$ , where the main targets are giants. In order to avoid the early type stars, we limit the stars

to have SSPP temperatures from 3000 K to 10 000 K and the signal-to-noise ratio larger than 10. We do not limit the low edge of  $\log g$ , but we note that our selected stars with SSPP parameters available in the SDSS database have surface gravity of  $\log g > 0.0$ . Fig. 3 shows the  $(g - r)_0$  versus CH(G) index for the above selected field stars with locations of member stars of M3 overplotted. It seems that most stars with  $(g - r)_0 > 0.4 \text{ mag}$  in our selected field sample are RGB stars and they match the locations of RGB stars of M3. In order to apply the method for further use, we have established a calibration between the CH(G) and  $(g - r)_0$  for RGB stars of  $CH(G) = 1.625(g - r)_0 - 1.174(g - r)_0^2 - 0.934$ . The dashed lines follow the above calibrated line with a deviation of 0.05 dex in the CH(G) index at a given  $(g - r)_0$  color. Stars within the dashed lines are classified as RGB stars. Stars significantly lower than the calibration may consist of early-AGB and RHB stars as indicated by member stars in M3. Turnoff and main sequence stars are clumped at the blue edge with  $(g - r)_0$  from 0.2 to 0.4 mag, they have CH(G) index lower than  $-0.50$ , and overlap with HB stars. RHB stars have a wider range of  $(g - r)_0$  from 0.2 to 0.5 mag but also have CH(G) indices less than  $-0.50$ .

### 3.2. Applying this method to $[\text{Fe}/\text{H}] \sim -2.3$

In order to extend the study to other metallicities, we investigated the spectroscopic data of the SDSS survey for M92 and M15, which have metallicities of  $[\text{Fe}/\text{H}] \sim -2.3$ . Fig. 4 shows the evolutionary stages, the CH(G) and S(3839) indices as a function of  $(g - r)_0$ , and the absolute magnitude versus S(3839) index. The same symbols as in Fig. 1 are used and turnoff stars from the GCs are shown as crosses. The same results are found at this metallicity but the scatter is slightly larger than that in M3. Specifically, the only possible AGB star is located at the lower edge in the diagram of the  $(g - r)_0$  versus CH(G) index, and subgiants and turnoff stars generally have lower CH(G) indices than those of RGB stars. In particular, a few stars with enhanced S(3839) indices lie in the middle part of the  $(g - r)_0$  versus CH(G) index diagram among member stars. Thus, the S(3839) index is not taken into account in selecting RGB stars in the following sections. Note that the deviation in the CH(G) index is large for one RGB star with the plate-mjd-fiberid numbers of 1960-53289-530 and the reason for this odd value is unknown.

In connection with possible differences between cluster and field stars, there are more cluster stars than field stars at the red end of RGB stars in M3 (see Fig. 3), which are lacking in M15/M92 (see Fig. 5). The difference in stellar color distribution between cluster and field stars comes from the target selection of the clusters in the SDSS spectroscopic survey because stars within the cluster tidal radius are favorably selected as targets and thus the

color range of the targets depends on the distance of the cluster. This selection criterion is not applied in the target selection of the general field. In addition, there is a hint that the CH(G) band index for field stars are slightly higher than those of the cluster stars at a given color in Fig. 5 and possibly in the blue end of RGB stars in Fig. 3. This discrepancy comes from the different absolute magnitudes of the stars in the sense that bright field stars with  $g_0 < 16 \text{ mag}$  show a slightly higher CH(G) band index than that of fainter stars with  $g_0 > 19 \text{ mag}$  in Fig. 5. The quality in the spectra of cluster stars is higher than the average value of field stars at the blue end of RGB stars (and also fainter magnitude), which leads to a slightly lower CH(G) index. In addition, the uncertainty in reddening for field stars could be larger than that of cluster stars, which could also contribute to the larger scatter (via  $(g-r)_0$  color) for field stars as compared with cluster stars in this diagram.

In a similar procedure as for M3, we selected a sample of field stars from the SDSS DR9 database with a  $(g-r)_0$  range of 0.1 to 0.8 *mag*,  $[\text{Fe}/\text{H}]$  from  $-2.4$  to  $-2.2$  dex and *logg* less than 3.5 dex, and the  $(g-r)_0$  versus CH(G) index diagram is shown in Fig. 5. The member stars from M92 and M15 are overplotted. Then we established a calibration for the selected field stars located in the RGB region of Fig. 5. We found that the coefficients are very similar to those at  $[\text{Fe}/\text{H}] = -1.5$ , but the constant is different. We thus adopted the same  $(g-r)_0$  coefficients and obtained the calibration of  $CH(G) = 1.625(g-r)_0 - 1.174(g-r)_0^2 - 0.982$  for  $[\text{Fe}/\text{H}] = -2.3$  as shown with the solid line in Fig. 5. Again, the two dashed lines show the locations of RGB stars around the calibration with a deviation of 0.05 *mag* in the CH(G) index at a given  $(g-r)_0$  color, and stars within the dashed lines are classified as RGB stars. In the selection, many CEMP stars (see later discussions in Sect. 3.3) with significant enhancement of the CH(G) index were avoided with the upper cut of the RGB calibration, and a few early-AGB stars or AGB-related stars are excluded with the low cut of the RGB calibration. Finally, it may be more reasonable to exclude blue stars where the strength of the CH(G) index starts to decrease for turnoff stars and RHB stars.

### 3.3. The metallicity-dependent calibration for RGB stars

In view of similar coefficients but different constants in the calibrations between  $(g-r)_0$  and CH(G) index at  $[\text{Fe}/\text{H}] = -1.5$  and  $[\text{Fe}/\text{H}] = -2.3$ , we attempt to establish a metallicity-dependent constant for the calibration. For this purpose, we need to extend and obtain constants for more metallicity bins. First, we selected field stars with  $(g-r)_0$  of 0.1 to 1.0 *mag* and *logg* less than 3.5 dex for each metallicity bin ranging from  $[\text{Fe}/\text{H}] < -2.8$  to  $[\text{Fe}/\text{H}] = 0.0$  with a step of 0.2 dex. We assume that the main populations of field stars, selected based on  $(g-r)_0$  of 0.4 to 1.0 *mag* and *logg* less than 3.5 dex at a given metallicity, are RGB stars in

the SDSS DR9 database. This assumption is valid for  $[\text{Fe}/\text{H}] = -1.5$  and  $[\text{Fe}/\text{H}] = -2.3$  as described above. Again, CEMP stars with significant enhancement of the  $\text{CH}(G)$  index at a given color and metallicity were avoided and we excluded blue stars with  $(g-r)_0 < 0.4$  being turnoff stars or RHB/BHB stars. Then we used the above-adopted coefficients for  $(g-r)_0$  and obtained a set of different constants for the individual metallicity bins in the fitting of RHB stars. Then we fit the constants with a metallicity-dependent linear function, and the final calibration gives  $\text{CH}(G) = 1.625(g-r)_0 - 1.174(g-r)_0^2 + 0.060[\text{Fe}/\text{H}] - 0.844$ .

Fig. 6 shows the location of selected RGB stars around the calibration (the solid line for  $[\text{Fe}/\text{H}] \leq -1.2$  and long dashed line for  $[\text{Fe}/\text{H}] > -1.2$ ) within the deviation of  $0.05 \text{ mag}$  (the two dashed lines for  $[\text{Fe}/\text{H}] \leq -1.2$ ). Note that we only show the ranges of  $(g-r)_0 = 0.1-0.8$  for  $[\text{Fe}/\text{H}] \leq -1.2$  and of  $(g-r)_0 = 0.1-1.0$  for  $[\text{Fe}/\text{H}] > -1.2$ , corresponding to GK giants. There are small numbers of stars outside the red cuts until M giants become significant at the metal-rich end. We should keep in mind that this calibration is only one possible way to select most RGB stars from the SDSS database. It is by no means the only solution to pick out RGB stars. In particular, this calibration deviates from the centering points of field giant stars and it gives too high values for the high metallicity end and perhaps too low values for the low metallicity end. We have thus provided an additional calibration of  $\text{CH}(G) = 0.953(g-r)_0 - 0.655(g-r)_0^2 + 0.060[\text{Fe}/\text{H}] - 0.650$  for  $[\text{Fe}/\text{H}] > -1.2$  to fit especially the high metallicity data in a better way. The solid line and two dashed lines for in Fig. 6  $[\text{Fe}/\text{H}] > -1.2$  is the new calibration and its deviation by the order of  $0.05 \text{ mag}$ . This new calibration may be more reasonable in view of the fact that the color range of RGB stars is shifted to the red end as the metallicity increases and the age span in field stars become very large for  $[\text{Fe}/\text{H}] > -0.5$ . Despite the possible deviation between the two calibrations at the high metallicity end, most field giant stars can successfully be picked out by selecting stars within a deviation of  $0.05 \text{ mag}$  in the  $\text{CH}(G)$  index from both calibrations. A catalog of the selected RGB stars are published electronically and a sample table consisting of the first ten stars is presented in Table 1.

Note that there is an interesting group of stars with significantly higher  $\text{CH}(G)$  index mainly at the blue end in the  $(g-r)_0$  versus  $\text{CH}(G)$  diagram in Fig. 6. There are 25 stars (stellar parameters and  $\text{CH}(G)$  indices are presented in Table 2) in our sample with carbon abundances available in Aoki et al. (2012) based on high resolution spectra for extremely metal poor stars selected from the SDSS survey. We overplotted the common stars in Fig. 6 according to the carbon to iron ratio ( $[C/Fe]$ ). It is clear that carbon enhanced metal poor (CEMP) stars with  $[C/Fe] > 1.0$  (open diamonds) based on the definition of Beers & Christlie (2005) are located in the upper part while stars with  $[C/Fe] < 1.0$  (open triangles) follow our selection regions of RGB stars. The only exception is the star 2183 – 53536 – 175 (plate-mjd-fiberid) (with additional open square in Fig. 6), which has

$[C/Fe] = 1.24$  but the spectra shows a weak CH(G) index. We suspected a too low  $[Fe/H]$  was obtained in Aoki et al. (2012) and the  $[C/Fe]$  reduces to 0.74 if the metallicity from SSPP catalog was used. Further study on this discrepancy is desirable for this star. Without the carbon abundances in our work, it is impossible to obtain the fraction of CEMP stars among normal stars. Alternatively, we selected stars with CH(G) index above  $-0.47$  for  $(g-r)_0 < 0.3$  and  $0.1$  mag higher than the RGB calibration for  $0.3 \leq (g-r)_0 \leq 0.8$  as being candidates of high branch CEMP stars, the fraction of which is 16% for  $[Fe/H] < -2.8$  and decreases to 5% at  $[Fe/H] = -2.0$ . This former value is lower than the fraction of 20% in Carollo et al. (2012) for  $[Fe/H] < -2.5$ , the value of 23% for  $[Fe/H] < -3.0$  in Yong et al. (2012) and the value of 28% in Norris et al. (2012) for  $[Fe/H] < -3.1$ . Note that our selection of high branch CEMP stars may reflect the definition of  $[C/Fe] > 1.0$  from Beers & Christlie (2005), while Norris et al. (2012) adopted the division of  $[C/Fe] > 0.7$  from Aoki et al. (2007). In addition, our fractions are based on evolved stars with SSPP  $logg < 3.5$ , while Carollo et al. (2012) include unevolved stars. In view of the two factors, our value is actually not inconsistent with those in the literature.

#### 4. Summary

We have measured the CH(G) index for evolved stars in M3 at  $[Fe/H] = -1.5$  and found a clear separation between red giant stars and early-AGB stars at similar colors. The calibration of the  $(g-r)_0$  versus CH(G) index is established to be  $CH(G) = 1.625(g-r)_0 - 1.174(g-r)_0^2 - 0.934$  based on field stars selected from the SDSS DR9 database with  $0.1 \leq (g-r)_0 \leq 0.8$ ,  $-1.6 \leq [Fe/H] \leq -1.4$  and  $logg < 3.5$ . With similar coefficients but a different constant of  $-0.982$ , the calibration can be established for  $[Fe/H] = -2.3$ . Stars selected from the two calibrations within a deviation of  $0.05$  mag in the CH(G) index at a given  $(g-r)_0$  color agree well with the locations of RGB member stars of M3 and M15/M92. We thus extended this kind of fitting to other metallicity bins, and the calibration of  $CH(G) = 1.625(g-r)_0 - 1.174(g-r)_0^2 + 0.060[Fe/H] - 0.844$  fits well the location of RGB stars for  $-3.0 < [Fe/H] \leq -1.2$ , but a new calibration of  $CH(G) = 0.953(g-r)_0 - 0.655(g-r)_0^2 + 0.060[Fe/H] - 0.650$  for  $-1.2 < [Fe/H] < 0.0$  seems to be more reasonable to select RGB stars from evolved stars. Note that these calibrations are obtained from the SDSS data set and they may not valid for other data sets because band strength indices are susceptible to the overall shape of the spectrum.

We provide an online table for the selected RGB stars. In the near future, we plan to apply this calibration to select RGB stars from the SDSS DR9 data set and investigate the chemical and kinematical properties (mainly based on radial velocities) of the Galaxy. This

kind of stellar tracer can extend to a distance of at least 20 kpc, which is further than the distance limit of 5 kpc using dwarfs in the SDSS survey.

We thank the referee for providing very good suggestions, which greatly improved the paper. This study is supported by the National Natural Science Foundation of China under grants No. 11233004, 11222326, 11073026, 11150110135, 11078019 and 11103034.

Funding for SDSS-III has been provided by the Alfred P. Sloan Foundation, the Participating Institutions, the National Science Foundation, and the U.S. Department of Energy Office of Science. The SDSS-III web site is <http://www.sdss3.org/>. SDSS-III is managed by the Astrophysical Research Consortium for the Participating Institutions of the SDSS-III Collaboration including the University of Arizona, the Brazilian Participation Group, Brookhaven National Laboratory, University of Cambridge, University of Florida, the French Participation Group, the German Participation Group, the Instituto de Astrofísica de Canarias, the Michigan State/Notre Dame/JINA Participation Group, Johns Hopkins University, Lawrence Berkeley National Laboratory, Max Planck Institute for Astrophysics, New Mexico State University, New York University, Ohio State University, Pennsylvania State University, University of Portsmouth, Princeton University, the Spanish Participation Group, University of Tokyo, University of Utah, Vanderbilt University, University of Virginia, University of Washington, and Yale University.

## REFERENCES

- Abazajian K.N., Adekman-McCarthy J.K., Agueros M.A., et al. 2009, *ApJS* 182, 543
- Aihara H., Allende Prieto C., An D., et al. 2011, *ApJS* 193, 29
- Ahn C., Alexandroff R., Allende Prieto C., et al. 2012, *ApJS*, 203, 21
- Allende Prieto, C., Beers, T. C., Wilhelm, R., et al. 2006, *ApJ*, 636, 804
- An D., Johnson J.A., Clem J.L. et al. 2008, *ApJS*, 179, 326
- Angelou G.C., Church R.P., Stancliffe R.J., Lattanzio J.C., Smith G.H., 2011, *ApJ*, 728, 79
- Aoki, W., Beers, T. C., Christlieb, N., Norris, J. E., Ryan, S. G., & Tsangarides, S. 2007, *ApJ*, 655, 492
- Aoki, W., Beers, T. C., Lee, Y.S., et al. 2012, *AJ*, in press (astro-ph/1210.1946)
- Beers, T. C., & Christlieb, N. 2005, *ARA&A*, 43, 531

- Briley M.M., Bell R.A., & Hoban S. 1990, ApJ, 359, 307
- Bond, N.A., Ivezić, Z., Sesar, B. et al. 2010, ApJ, 718, 1
- Carollo, D., Beers, T.C., Chiba, M. et al. 2010, ApJ, 712, 692
- Carollo, D., Beers T.C., Bovy J. et al. 2012, ApJ, 744, 195
- Dotter A., Chaboyer B., Jevremovic D., Kostov V., Baron E., Ferguson J.W., 2008, ApJS, 178, 89
- Eisenstein D.J., Weinberg D.H., Agol E., et al. 2011, AJ 142, 72
- Harris W.E. 1996, AJ, 112, 1487
- Lee S.G., 1999, AJ, 118, 920
- Lee Y.S., Beers T.C., Sivarani T. et al. 2008, AJ, 136, 2022
- Lee Y.S., Beers T.C., Sivarani T. et al. 2008, AJ, 136, 2050
- Norris J., Cottrell P.L., Freeman K.C., Da Costa G.S. 1981, ApJ, 244, 205
- Norris J., Yong D., Bessell M.S. et al. 2012, astro-ph/12113157
- Palladino L.E., Holley-Bockelmann K, Morrison H., et al. 2012, AJ, 143, 128
- Smolinski J.P., Lee Y.S., Beers T.C., et al. 2011, AJ, 141, 89
- Smolinski J.P., Martell S.L., Beers T.C., Lee Y.S. 2011, AJ, 142, 126
- Suntzeff N.B. 1981, ApJS, 47, 1
- Sweigart A.V., & Mengel J.G. 1979, ApJS, 229, 624
- Yanny B., Rockosi C., Newberg H.J., et al. 2009, AJ, 137, 4377
- Yong D., Norris J., Bessell M.S. et al. 2012, astro-ph/12083016
- Zinn R., 1973, ApJ, 182, 183

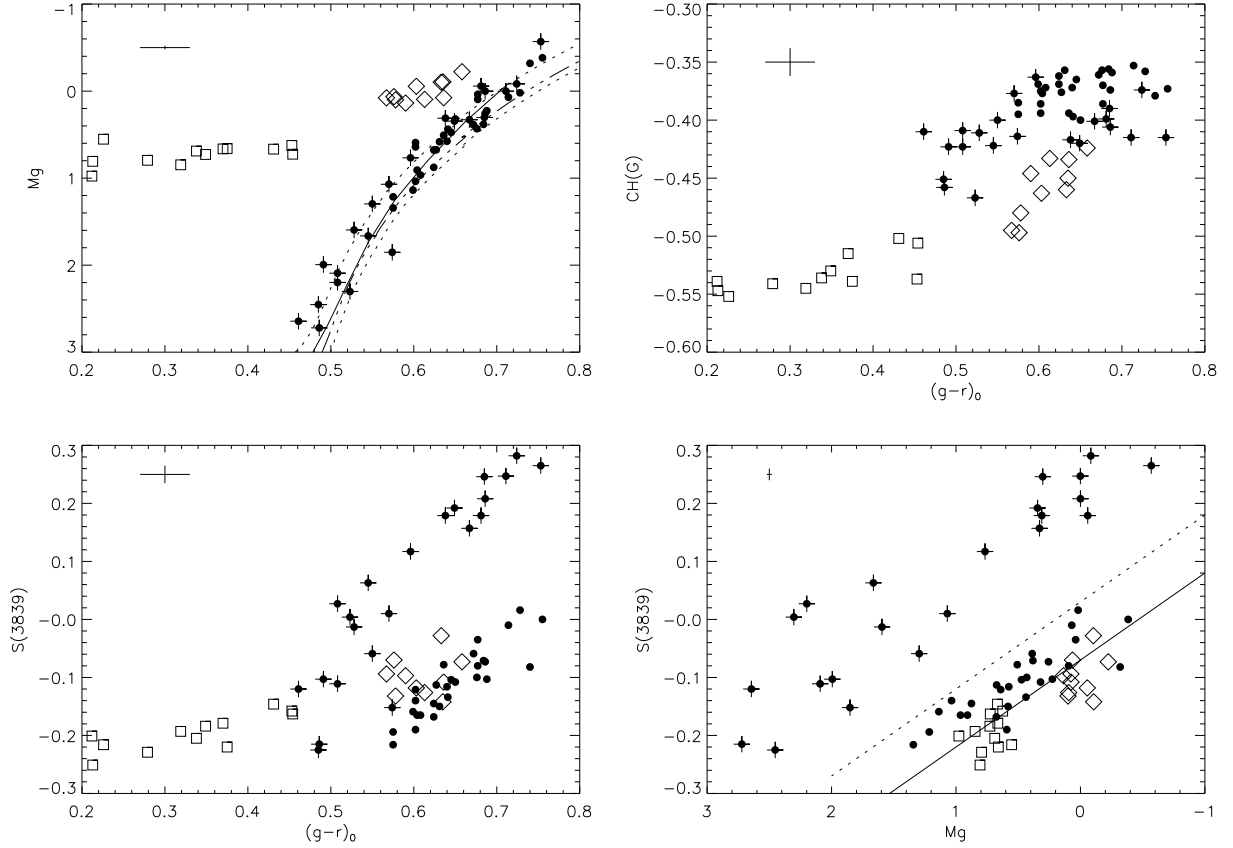


Fig. 1.— Upper panels: The absolute magnitude  $M_g$  and the CH(G) index as a function of  $(g-r)_0$  for RHB (squares), early-AGB (diamonds), and RGB (filled circles) stars in M3. The solid line is the observed FS of An et al. (2008) and the dashed lines show theoretical isochrones of 8, 11.5 and 14 Gyr at  $[\text{Fe}/\text{H}] = -1.5$  from Dotter et al. (2008). Lower panels: The S(3839) indices are shown as functions of  $(g-r)_0$  and the absolute magnitude  $M_g$  for stars in M3. The solid line shows the fit to S(3839)-normal stars and the S(3839)-enhanced stars above the dashed line are plotted with additional pluses in all panels.

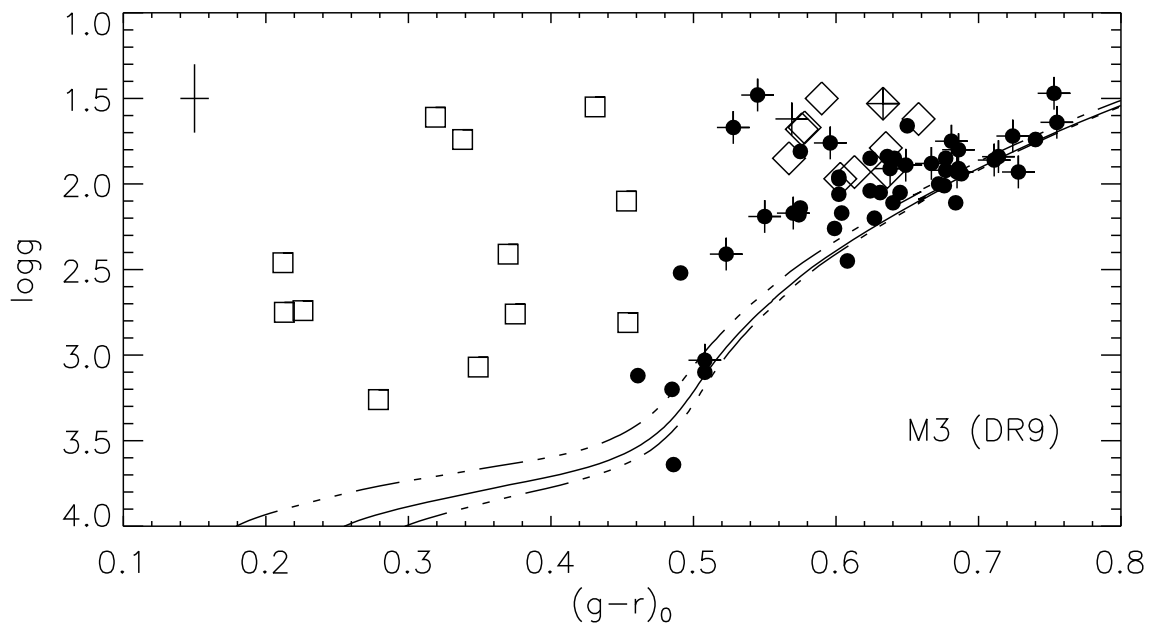
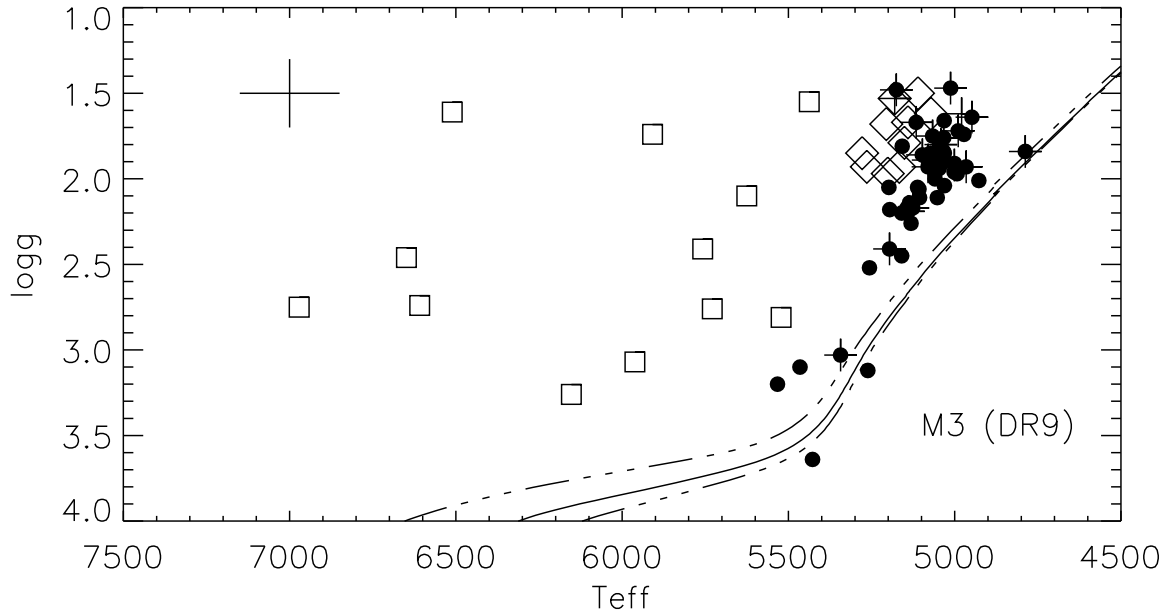


Fig. 2.— The  $T_{eff}$  versus  $\log g$  diagram for member stars in M3. The symbols are the same as in Fig. 1.

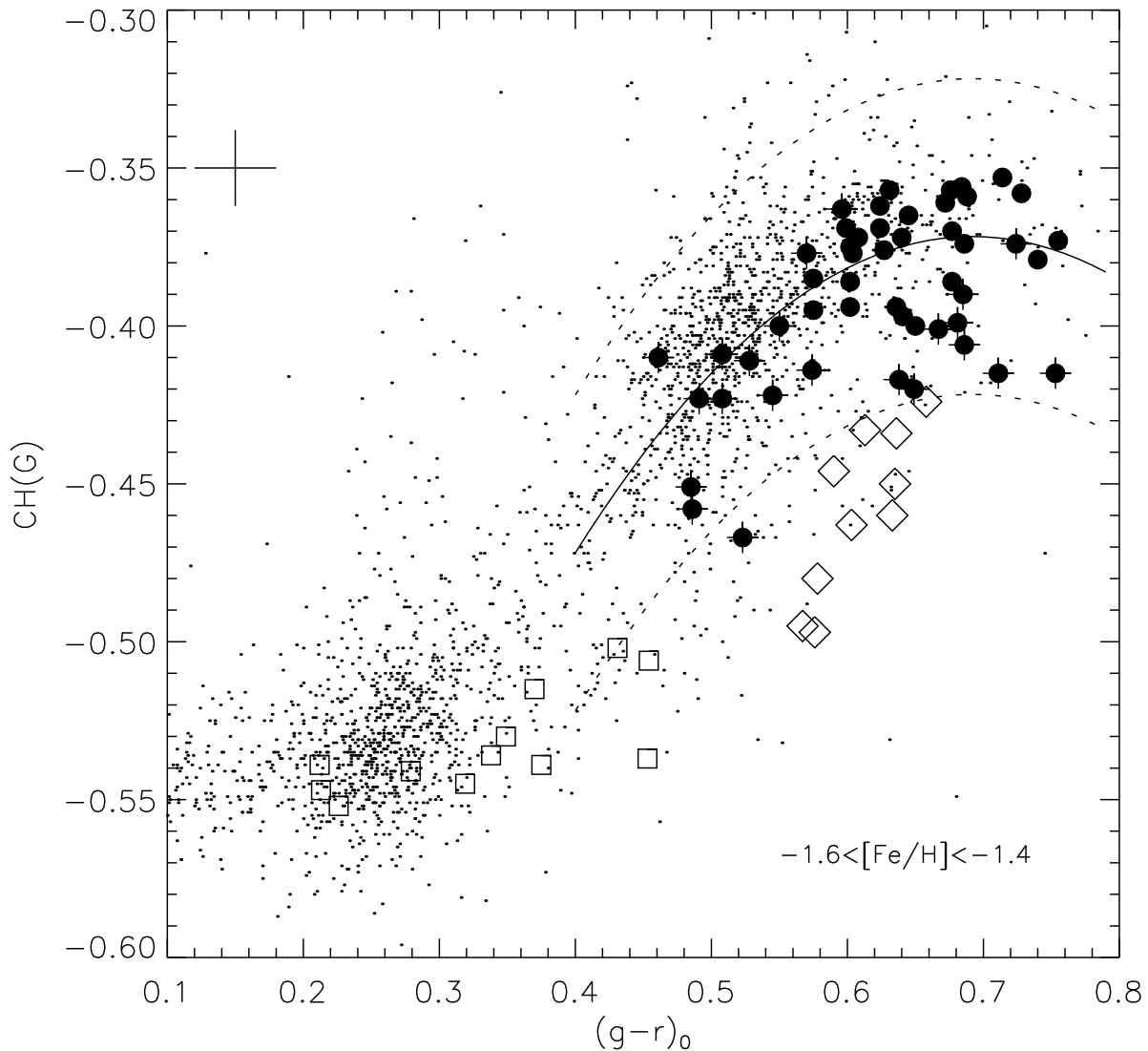


Fig. 3.— The  $(g-r)_0$  versus  $CH(G)$  index for field stars with  $0.1 \leq (g-r)_0 \leq 0.8$  mag,  $-1.6 \leq [Fe/H] \leq -1.4$  and  $\log g < 3.5$  in the SDSS DR9 catalog (small dots). Member stars from M3 are indicated with the same symbols as in Fig. 1. The calibration of  $CH(G) = 1.625(g-r)_0 - 1.174(g-r)_0^2 - 0.934$  and the deviations of  $0.05$  mag are indicated by solid and dashed lines. Stars within the dashed lines are classified as RGB stars.

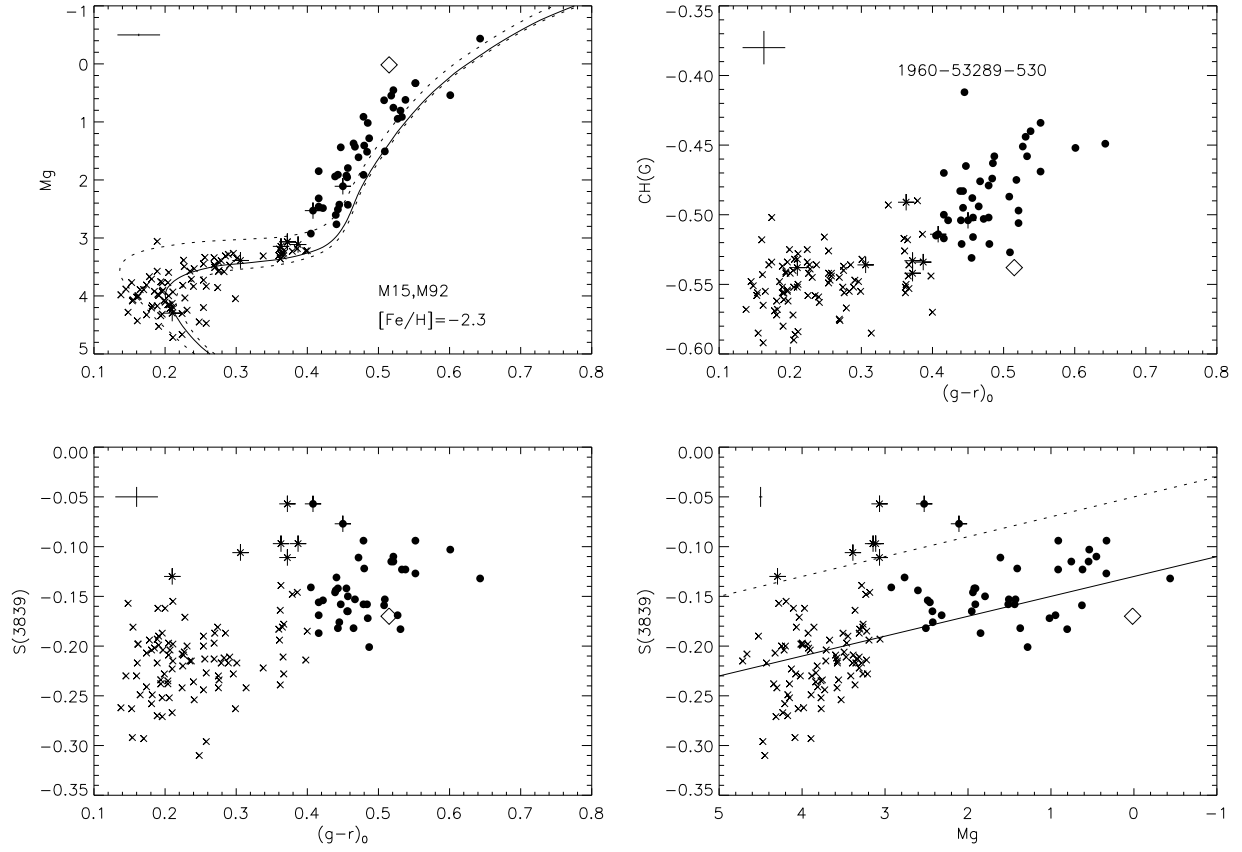


Fig. 4.— The CH(G) and S(3839) indices versus  $M_g$  and  $(g-r)_0$  for member stars in M92 and M15 with  $[Fe/H] \sim -2.3$ . Turnoff and subgiant stars are indicated by crosses and other symbols are the same as in Fig. 1.

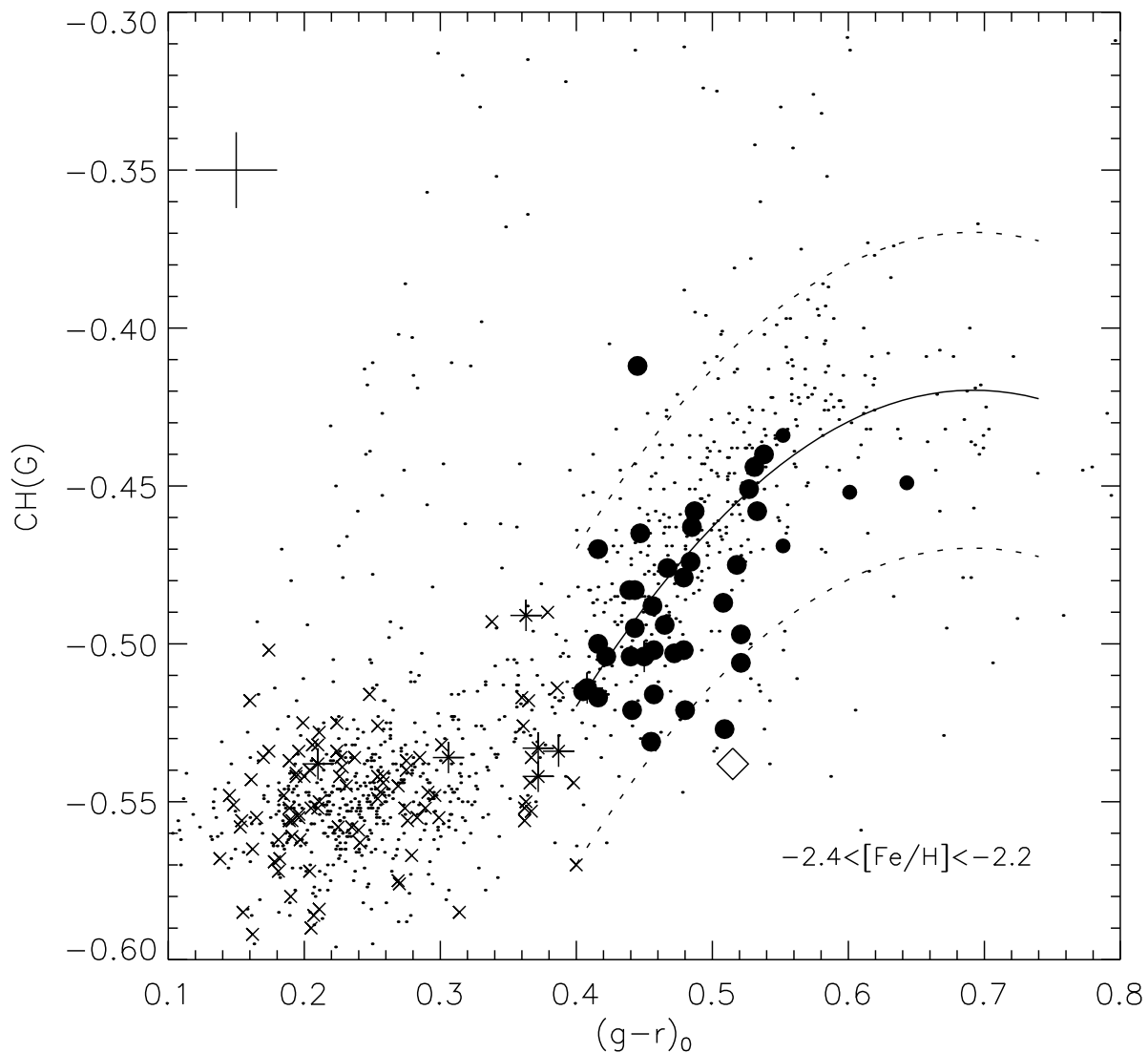


Fig. 5.— The  $(g-r)_0$  versus  $CH(G)$  index diagram for field stars with  $[Fe/H] = -2.4$  to  $-2.2$ ,  $(g-r)_0$  of 0.1 to 0.8 *mag* and  $\log g$  less than 3.5 dex in the SDSS DR9 database. Member stars from M92 and M15 with  $[Fe/H] \sim -2.3$  are overplotted. The calibration of  $CH(G) = 1.625(g-r)_0 - 1.174(g-r)_0^2 - 0.982$  is shown with the solid line, and stars within the deviations of 0.05 *mag* (dashed lines) are classified as RGB stars.

Table 1: The first ten stars in the selected RGB sample.

plate	mjd	fiber	[Fe/H]	$(g - r)_0$	CH(G)
2669	54086	534	-3.03	0.564	-0.452
2724	54616	324	-3.15	0.636	-0.485
2271	53726	2	-3.15	0.460	-0.555
1664	52965	452	-3.06	0.441	-0.543
2547	53917	163	-3.04	0.456	-0.503
2534	53917	546	-3.26	0.622	-0.422
2553	54631	439	-3.00	0.446	-0.500
2186	54327	277	-3.06	0.468	-0.540
2302	53709	182	-3.55	0.544	-0.509
2300	53682	472	-3.01	0.607	-0.417

Table 2: The SDSS identifications, plate-mjd-fiberid numbers, stellar parameters and  $[C/Fe]$  from Aoki et al. (2012), stellar parameters from SDSS DR9 database and CH(G) indices from this work for 25 common stars are presented.

SDSS ID	plate-mjd-fid	Teff	logg	[Fe/H]	[C/Fe]	Teff	logg	[Fe/H]	CH(G)
		HRS	HRS	HRS	HRS	DR9	Dr9	Dr9	this
SDSS J0002+2928	2803-54368-459	6150	4.0	-3.26	2.63	6239	3.33	-2.879	-0.414
SDSS J0018-0939	1912-53293-352	4600	5.0	-2.65	-0.88	4601	3.38	-3.012	-0.460
SDSS J0126+0607	2314-53713-090	6900	4.0	-3.01	3.08	6799	3.88	-2.860	-0.475
SDSS J0259+0057	1513-53741-338	4550	5.0	-3.31	0.02	4578	3.64	-3.704	-0.401
SDSS J0308+0505	2335-53730-314	5950	4.0	-2.19	2.36	5961	3.14	-2.423	-0.313
SDSS J0351+1026	2679-54368-543	5450	3.6	-3.18	1.55	5631	3.02	-2.773	-0.387
SDSS J0711+6702	2337-53740-564	5350	3.0	-2.91	1.98	5396	2.17	-2.914	-0.280
SDSS J0723+3637	2941-54507-222	5150	2.2	-3.32	1.79	5076	2.65	-3.480	-0.328
SDSS J0741+6708	2939-54515-414	5200	2.5	-2.87	0.74	5252	1.96	-2.965	-0.445
SDSS J0858+3541	2380-53759-094	5200	2.5	-2.53	0.30	5150	1.92	-2.885	-0.472
SDSS J0912+0216	0471-51924-613	6150	4.0	-2.68	2.05	6208	3.38	-2.545	-0.440
SDSS J1036+1212	1600-53090-378	5850	4.0	-3.47	1.84	5847	2.86	-3.307	-0.518
SDSS J1241-0837	2689-54149-292	5150	2.5	-2.73	0.50	5160	2.57	-2.745	-0.395
SDSS J1242-0336	2897-54585-210	5150	2.5	-2.77	0.64	5078	2.48	-3.065	-0.444
SDSS J1245-0738	2689-54149-491	6100	4.0	-3.17	2.53	6212	2.97	-2.894	-0.392
SDSS J1349-0229	0913-52433-073	6200	4.0	-3.24	3.01	6168	4.39	-3.163	-0.373
SDSS J1422+0031	0304-51609-528	5200	2.2	-3.03	1.70	5181	3.03	-3.248	-0.345
SDSS J1612+0421	2178-54629-546	5350	3.3	-2.86	0.63	5349	2.49	-3.194	-0.520
SDSS J1613+5309	2176-54243-614	5350	2.1	-3.33	2.09	5451	2.70	-2.853	-0.337
SDSS J1626+1458	2202-53566-537	6400	4.0	-2.99	2.86	6416	3.38	-2.542	-0.442
SDSS J1646+2824	1690-53475-323	6100	4.0	-3.05	2.52	6172	3.20	-2.688	-0.383
SDSS J1703+2836	2808-54524-510	5100	4.8	-3.21	0.28	5065	3.48	-3.537	-0.463
SDSS J1734+4316	2799-54368-138	5200	2.7	-2.51	1.78	5025	1.98	-3.177	-0.250

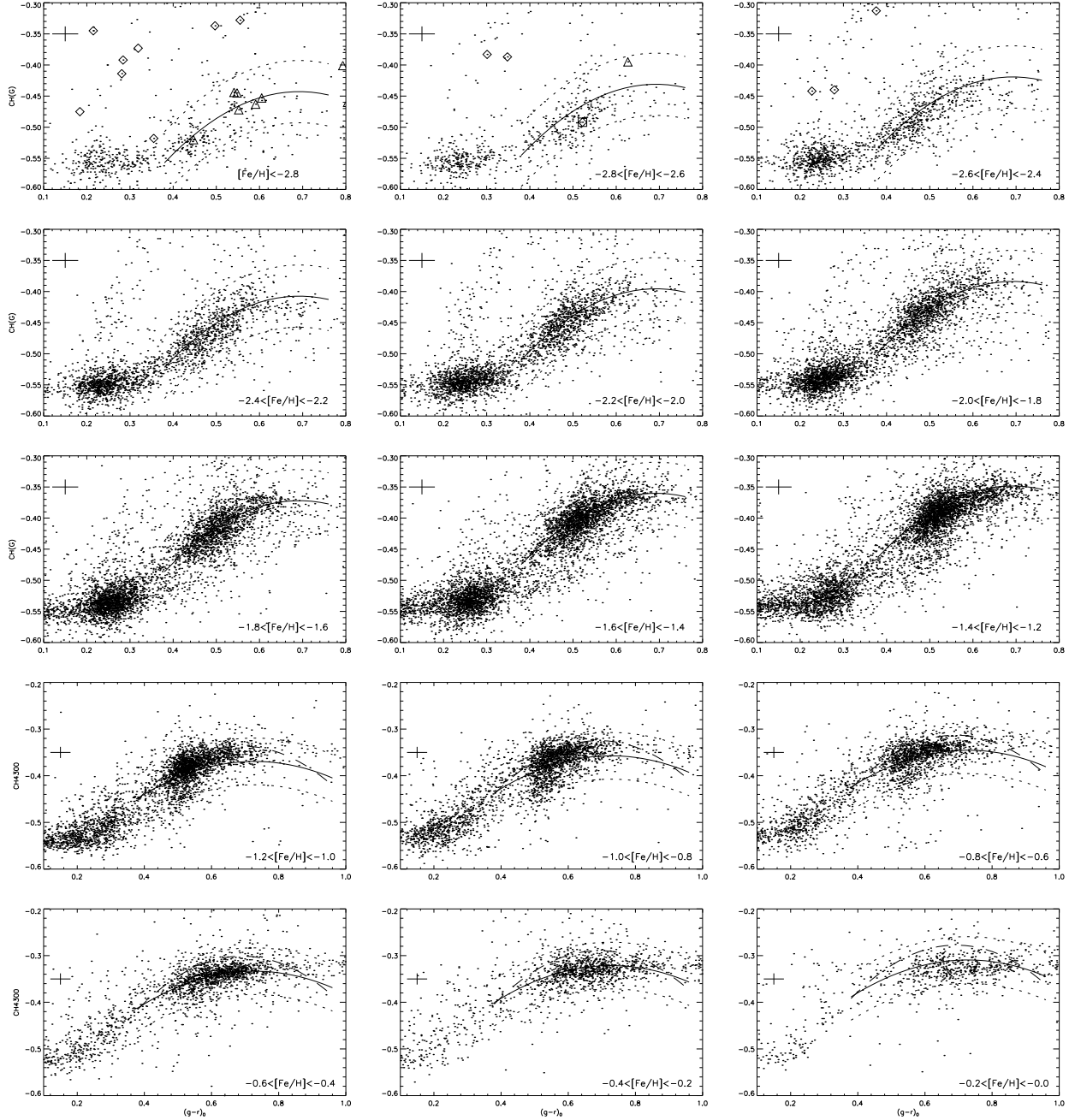


Fig. 6.— The  $(g-r)_0$  versus  $CH(G)$  index diagram from  $[Fe/H] < -2.8$  to  $[Fe/H] = 0.0$  with a bin of 0.2 dex. The suitable calibration and the selection ranges for RGB stars in a given metallicity bin are indicated by the solid and dashed lines, respectively. For stars with  $[Fe/H] > -1.2$  the solid lines are based on the new calibration of  $CH(G) = 0.953(g-r)_0 - 0.655(g-r)_0^2 + 0.060[Fe/H] - 0.650$ , while the long dashed lines are based on the same calibration of  $CH(G) = 1.625(g-r)_0 - 1.174(g-r)_0^2 + 0.060[Fe/H] - 0.830$  as that of  $[Fe/H] \leq -1.2$  stars. Stars with  $[C/Fe] > 1.0$  from Aoki et al. (2012) are indicated by open diamonds and stars with  $[C/Fe] < 1.0$  are shown as open triangles. The exceptional star with  $[C/Fe] = 1.24$  is shown by additional open square. Note that two stars with the  $CH(G)$  index lower than  $-0.3$  are outside of the first panel.